Cement and Concrete Research 110 (2018) 1–12

Contents lists available at ScienceDirect

Cement and Concrete Research

journal homepage: www.elsevier.com/locate/cemconres

The origin, composition and early age hydration mechanisms of Austrian natural Portland cement

Farkas Pintér[a,*], Christophe Gosselin[b]

[a] Scientific Laboratory, Federal Monuments Authority Austria, Arsenal 15/4, A-1030 Vienna, Austria
[b] Geotest SA, En Budron E7, CH-1052 Le Mont-sur-Lausanne, Switzerland

ARTICLE INFO

Keywords:
Portland cement (D)
Cement manufacture (E)
Hydration products (B)
SEM-EDX (B)
Petrography (B)

ABSTRACT

The chemical and mineralogical properties of cement residues and hydration products have been assessed in historical Portland cement mortars. Results indicate a long time of burning and residence and a slow cooling rate. C_2AS, CS and under burned raw material residues suggest inhomogeneous heat distribution typical for shaft kilns. Additionally, minor amounts of $\$-C_2S$, $C_5S_2\$$, $C_4A_3\$$ and CaS refer to the burning of a pyrite-bearing marlstone and a brown coal used as a solid fuel. Monosulfoaluminate intermixed with monocarboaluminate predominantly concentrate in the inner hydration products confirming the absence of interground calcium sulfate as a retarding agent. The distribution of AFm phases suggests the dissolution of sulfur from the sulfur-bearing cement residues and subsequent carbonation in the later stage of hydration. The coarse grain size of the cement and the presumable application of a historical deactivation method resulted in the formation of high microporosity.

1. Introduction

The evolution of calcareous hydraulic binders during the course of the 19th century was a consequence of numerous experiments and developments carried out starting in the 1750s [1,2]. These efforts achieved not only the production of watertight binders, but also materials exhibiting higher strength compared to traditional hydraulic mortars based on pozzolanic lime [1]. The first products of these trials were Natural Hydraulic Lime (NHL, 1756) and Roman cement (RC, 1796), which can be considered as the direct precursors of early Portland cements [3,4]. The continuous development of Portland cement (PC) started in the 1840s with William Aspdin's and especially Isaac Johnson's awareness of the importance of sufficiently high temperature during calcination [1,2]. These early, or also called, meso-PCs [1,2] represented heterogeneous materials containing calcium silicate products formed around or slightly above the temperature of sintering, but also phases formed in lower temperature regimes very similar to those found in NHL or RCs [3,5].

Later in the 1870–80s the implementation of continuous shaft kilns, an important factor in the technological development of PC along with the adoption of early standards, led to an increase of quality and quantity of PC production [1–3]. At the turn of the 20th century the increasing requirements of the construction industry [3], along with the introduction of rotary kilns, ball mills and the use of calcium sulfate as a retarding agent, made PC the most widely used hydraulic binder and building material in the world.

While most European cement manufacturers produced their own early PCs by using artificially by-mixed raw materials (i.e. lime and clay), in Austria the first PC was produced by using a local marlstone as the single raw material at the Perlmoos cement plant in Kirchbichl near Kufstein, Tyrol in 1856 [6–8]. This “new cement” was accidentally discovered when residues of over burned clinker of the local RC plant were milled and applied as a mortar binder for a local construction site [7]. The awareness of the astonishingly good quality and much higher compressive strength of this binder compared to those of based on RC, led to further trials, the identification of the exact geological strata of the raw material and finally the beginning of the production of natural PC in Austria [7]. This natural meso-PC was produced similarly to RC: the coarsely crushed raw material containing calcium carbonate, silicate and aluminosilicate minerals in intimate mixture was calcined in vertical shaft kilns using the local brown coal as solid fuel [6,7]. Unlike RCs, however, the calcination temperature was higher and reached or exceed the heat of sintering (i.e. ~1300 °C), where free lime combines with C_2S to form C_3S. The exact mineralogical requirements for the production of good-quality cement meant that only restricted dissemination of natural PCs in Europe in the second half of the 1800s was possible. Based on historical data [6], only three Austrian cement plants and another one near the Black Sea produced natural PC on the

* Corresponding author.
E-mail addresses: farkas.pinter@bda.gv.at (F. Pintér), christophe.gosselin@geotest.ch (C. Gosselin).

https://doi.org/10.1016/j.cemconres.2018.04.020
Received 25 November 2017; Received in revised form 21 April 2018; Accepted 23 April 2018

Continent in the 19th century.

Currently environmental concerns related to cement production has encouraged studies of alternative binders, based on sustainable technology using local raw materials and moderate calcination processes. Beyond these environmental issues, there is a recent and increasing interest in investigating historic PC mortars and concretes due to their significant role in the civil engineering and architecture of the late 19th and the 20th century. Nevertheless, the literature [e.g. 9–17] remains rather sporadic on the mineralogical properties of these binders. Consequently, investigation into the material characteristics of historic objects made out of early PC supports the understanding of their often excellent performance after more than a century, which combined with the analysis of historic mortars and concrete may also contribute to the current development of alternative binders.

The present study deals with 19th century natural PC mortar samples applied at the neo-Gothic collegiate church of the Benedictine monastery of Admont, in Northern Styria, Austria. The original medieval church was reconstructed after a disastrous fire in 1865 [18]. The historical literature [18,19] as well as some unpublished original shipping documents from the former Perlmoos cement plant which produced natural PC in the 1860s and 70s [7], confirm that Perlmoos cement was used during the rebuilding of the church between 1866 and 1870. The study of the mortars was based on optical and electron microscopic techniques, in order to understand their production technology, hydration mechanisms and long-lasting performance.

2. Sampling and methods

Two cement mortars were selected from the building, dating to the reconstruction period in the late 1860s: a window ledge (ADM1) and a floral cast element (ADM2) at the northern façade. After a preliminary drying at 40 °C in a drying chamber, the samples were embedded in epoxy resin (Araldite 2020) to prepare thin sections and two series of polished sections. One series of polished sections was etched with Nital (1.5 ml of HNO_3 in 100 ml of isopropyl alcohol for approx. 7 s, and the residue of the etchant was removed by ethanol [5]). Samples were analyzed with the optical microscope (Zeiss AXIOScope A1) using reflected light (RL) for the etched polished sections and transmitted polarized light (TPL) for the thin sections, respectively. Non-etched polished sections were coated with carbon to be analyzed by scanning electron microscope (Philips Quanta 200, acceleration voltage 12 kV), coupled with an energy dispersive X-ray spectrometer (Bruker AXS Quantax). A large number of standardized analysis points and atomic ratio plots were used to characterize hydration products, residual cement grains and other binder-related phases in order to understand the burning conditions as well as the hydration process. The determination of cement minerals was carried out on the basis of the usual nomenclature used in the cement chemistry without the confirmation of exact crystalline polymorphs (e.g. by micro-diffraction techniques). The cement notation used throughout the document being: A = Al_2O_3, C = CaO, $\underline{C}$ = CO_3, F = Fe_2O_3, H = H_2O, M = MgO, S = SiO_2, and \$ = SO_3. The binder-to-aggregate ratios and the amount of air voids have been estimated by using the SEM-BSD images.

3. Results

3.1. General macro- and microscopic features

Both samples exhibited a compact structure free of macro cracks and a generally very good state of preservation. A beige-brown discoloration of the surface and the matrix (Fig. 1) is a common feature of early PCs and corresponds to carbonated [17] and/or to oxidised binder areas. The moderately well sorted, angular to rounded aggregates, with a size range of 0.1 to 1.5 mm and 0.1 to 3 for the samples ADM1 and ADM2, respectively, are predominantly of carbonate nature with low amounts of silicate components (Fig. 2). These aggregates suggest the use of alluvial deposits connecting to the local sediments of the nearby Enns River. The estimated b/a ratios are approx. 1 to 2.5-3 in both mortars. Irregular water voids up to 2 mm diameter are common in ADM1 (Fig. 3), while approx. 4% of homogenously distributed

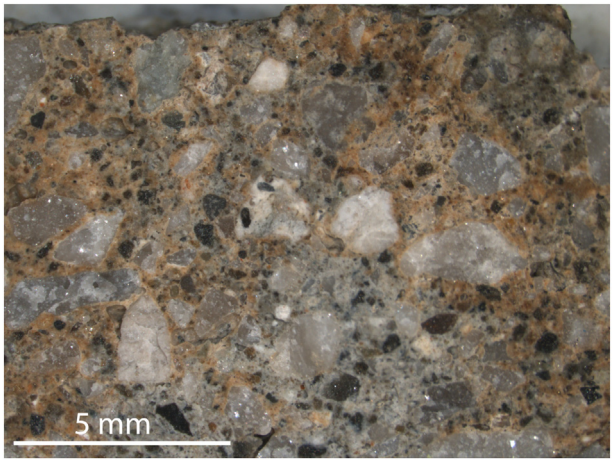

Fig. 1. Beige discoloration of the matrix on the broken surface (ADM2) (For interpretation of the references to color in this figure legend, the reader is referred to the web version of this article.).

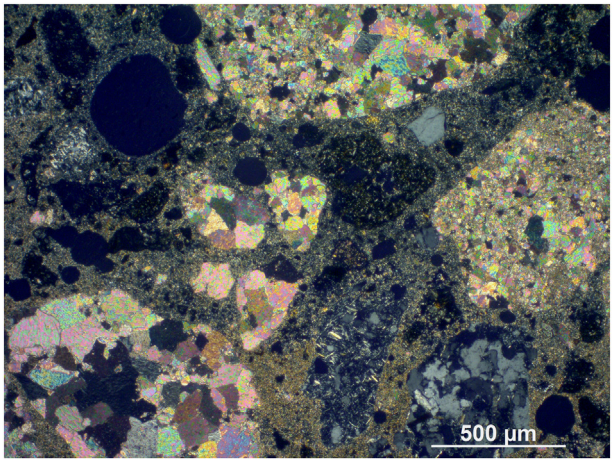

Fig. 2. Dolomite and polycrystalline quartz aggregates in the carbonated cement matrix (ADM1); TPL.

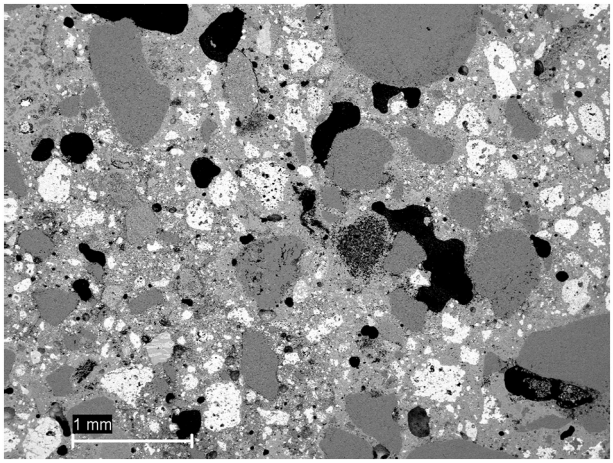

Fig. 3. Coarse residual cement (white) and irregularly shaped water voids (ADM1); SEM-BSD.

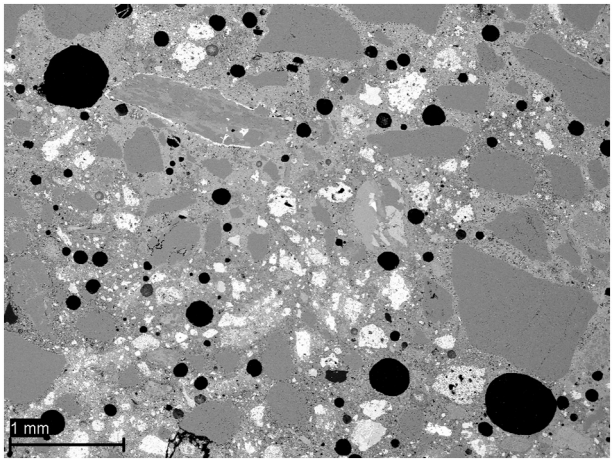

Fig. 4. Homogenously distributed entrapped air voids (ADM2); SEM-BSD.

entrapped air voids, characteristic for cast elements, are observed in the sample ADM2 (Fig. 4).

3.2. Characteristics of residual cement grains and other binder-related phases

The existence of heterogeneous and coarse residual cement grains is the most remarkable characteristics of historical PCs [1,5,13–16]. Unhydrated cement residues in ADM1 (Fig. 3) are slightly coarser compared to ADM2 (Fig. 4) ranging from 0.2 to 0.5 mm in diameter up to a maximum of 0.8 mm (sample ADM1). Based upon the detailed mineralogical observations from optical microscopy and SEM-EDX, the residues have been classified into four cement grain types (CGT1 to 4, Table 1).

This classification is common between the two samples which are discussed together.

Table 2 contains the chemical composition (given in atomic %) of characteristic examples of cement mineral phases.

3.2.1. Cement residues with PC character (CGT1)

Around three-fourths of the cement residues are classified as this type. The four main PC clinker minerals, namely C_3S, C_2S, aluminate and ferrite, are present (Fig. 5) similar to those in modern PCs, but their proportion, size and shape differ.

C_3S exhibits idiomorphic tabular to subhedral rounded or distorted crystals (Figs. 5 and 6) with less distinct margins and sometimes coalescent grains (Fig. 5). Their size varies between 10 and 80 μm (in average 40 to 60 μm). Several cement residues contain corroded C_3S grains surrounded by small secondary C_2S crystals (Fig. 6), with no evidence of CaO in these zones.

C_2S is more abundant than C_3S. Besides the typical round crystals (Fig. 7) frequently forming up to 0.5 mm large clusters, atypical large, elongated or wedge-like [15,16] shapes are also observed (Figs. 8 and 9). The grain size varies within a wide range of 5 to 80 μm, where the elongated types measure the largest sizes (up to 100 μm) and showing often a cleavage perpendicular to the elongation of the crystals (Figs. 8 and 9). Polysynthetic twinning exhibiting one set of parallel lamellae, typical for the type II C_2S [20], is predominantly observed in the wedge-shaped type (Fig. 8), while two sets of intersecting lamellae (type I, [20]) occur only in a few crystals. C_2S not presenting any clear lamellae, suggest the existence of type III [5]. Several crystals demonstrate reabsorbed or finger-like pattern within the flux phases (Fig. 10).

For a few of C_2S grains high amounts of Mg are incorporated, leading to an average composition $Ca_{24at\%}$, $Si_{14at\%}$ and $Mg_{3at\%}$, matching with that of the bredigite type mineral $Ca_7Mg(SiO_4)_4$ [21,22].

The ratio of flux phases is considerably higher compared to modern OPC, and aluminate dominates over ferrite. C_3A (with average atomic ratios of Ca/Al ~1.50) and ferrite (with average atomic ratios of Ca/(Al + Fe) ~0.90) have very large crystals filling the interstitial space between the calcium silicates (Figs. 5–10). Calcium aluminate exhibits another type having an average atomic ratio of Ca/Al ~0.85 corresponding to $C_{12}A_7$ (Fig. 7). MgO is observed as small subhedral crystals (Figs. 9 and 10).

3.2.2. Sulfur-bearing cement residues (CGT2)

Cement grains in which the minerals and solid solutions contain various amounts of SO_3, belong to the CGT2 group. While C_3S is detected only sporadically, C_2S exists both as dicalcium silicate, as the dominating phase free of sulfur and a sulfur-bearing type ($-$-C_2S) with an average chemical composition of $C_2S_{0.8}\$_{0.2}$ (Table 2) corresponding to a sulfur content of app. 3.7 wt%. A few of these phases contain isolated minute inclusions rich in iron and sulfur (Fig. 11). Fe to S atomic ratios of approx. 0.82 suggest the existence of the iron sulphide pyrrhotite ($Fe_{(1-x)}S$, X = 0 to 0.2). Minor impurities of Ca and Si (Table 2) are due to the very small grain size and the SEM interaction volume,

Table 1
Cement and binder-related grain types (CGT) identified in the samples (common: > 75%, rare: 10–20%, in traces < 5%).

CGT and its frequency among unhydrated residues	Characteristic mineral phases		Shape	Average size
CGT1 common	C_3S		Subhedral to euhedral	10 to 60 (max. 80) μm
	C_2S		Round	10 to 20 μm
			Elongated/wedge-shaped	20 to 80 (max. 100 μm)
	Aluminate	C_3A	Anhedral	up to 80 μm
		$C_{12}A_7$	Anhedral	up to 70 μm
	Ferrite		Anhedral	up to 80 μm
	MgO		Subhedral to euhedral	5 to 10 μm
CGT2 rare	C_2S		Round, rarely elongated	5 to 20 (max. 40 μm)
	$-$-C_2S		Anhedral	10 to 70 μm
	$C_5S_2\$$		Anhedral	up to 100 μm
	$C_4A_3\$$		Anhedral	up to 20 μm
	Aluminate		Anhedral	up to 150 μm
	Ferrite		Anhedral	up to 100 μm
	CaS		Anhedral droplets	1 to 5 μm
	(Mg,Fe)O		Subhedral to euhedral	5 to 10 μm
CGT3 in traces	CS		Subhedral to euhedral laths	20 to 100 μm
	Melilite (C_2AS)		Subhedral to euhedral laths	
CGT4 in traces	Residual silica (predominantly quartz) with rim of Ca diffusion		–	5 to 10 (max. 60 μm)
	Residues of the raw material incl. quartz, alkali-feldspar, mica, carbonates and pyrite in traces		–	200 to 500 μm

Table 2
Chemical composition given in atomic % of characteristic cement minerals in the different CGTs (EDX = spots of EDX measurements, see Figs. 5–19 for the exact positions).

	Phase		EDX	O	Na	Mg	Al	Si	S	K	Ca	Ti	Fe
CGT1	C_3S		+1	55.15	0.22	0.37	0.55	10.46	0.04	0.77	32.35	0.03	0.00
	C_2S	Round	+2	56.28	0.38	0.32	0.91	13.01	0.26	0.77	26.79	0.00	0.29
		Large, elongated	+3	56.69	0.26	0.38	0.74	13.68	0.14	0.86	26.79	0.04	0.15
	Aluminate	C_3A	+4	57.46	0.20	0.45	16.31	0.26	0.00	0.10	25.12	0.00	0.10
		$C_{12}A_7$	+5	55.82	0.70	0.70	22.68	0.37	0.14	0.17	19.26	0.00	0.17
	Ferrite		+6	55.93	0.35	1.63	9.61	0.88	0.00	0.37	18.84	0.73	11.64
	MgO		+7	50.02	1.40	47.26	0.05	0.21	0.04	0.00	0.16	0.00	0.86
CGT2	C_2S		+8	57.21	0.18	0.22	0.28	14.27	0.08	0.12	27.89	0.00	0.00
	$-$C$_2$S		+9	57.29	0.04	0.89	0.33	10.54	2.85	0.05	26.80	0.07	0.75
	$C_5S_2$$		+10	59.65	0.20	0.22	0.35	9.72	4.78	0.08	24.80	0.11	0.00
	$C_4A_3$$		+11	57.78	0.07	0.18	21.89	0.16	3.96	0.13	15.13	0.05	0.55
	Aluminate		+12	56.36	0.47	0.42	21.87	0.57	0.70	0.41	18.67	0.00	0.21
	Ferrite		+13	55.93	0.14	1.63	6.12	0.46	0.57	0.21	20.87	0.53	14.32
	$Fe_{(1-x)}S$		+14	12.20	0.00	0.00	0.00	3.05	42.96	0.00	6.20	0.00	35.17
	CaS		+15	0.00	0.00	0.08	0.00	0.00	51.37	0.00	48.24	0.00	0.04
	(Mg,Fe)O		+16	50.12	0.97	41.30	0.02	0.26	0.05	0.00	0.39	0.00	6.89
CGT3	CS		+17	60.80	0.09	0.14	0.21	19.42	0.00	0.50	18.84	0.00	0.00
	Glassy matrix		+18	63.50	0.8	2.44	5.78	18.02	0.02	1.32	7.39	0.05	0.68
CGT4	CS		+19	63.31	0.05	0.04	0.16	17.95	0.00	0.25	17.19	0.00	0.05
	C_2S		+20	56.75	0.53	0.35	0.48	13.52	0.12	0.72	27.05	0.00	0.29

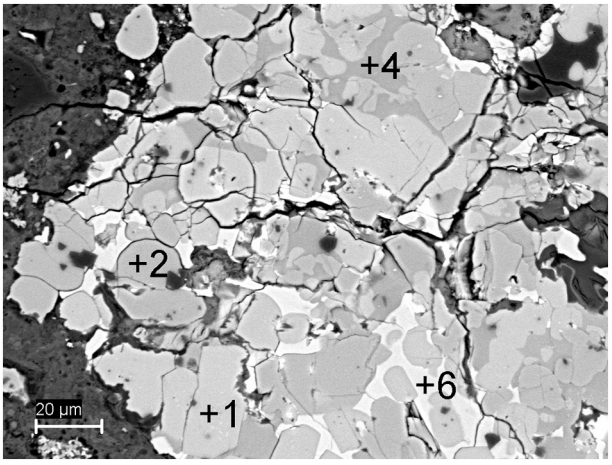

Fig. 5. CGT1: coarse residual cement grain with coalescent C_3S (+1), C_2S (+2), C_3A (+4) and ferrite (+6); SEM-BSD.

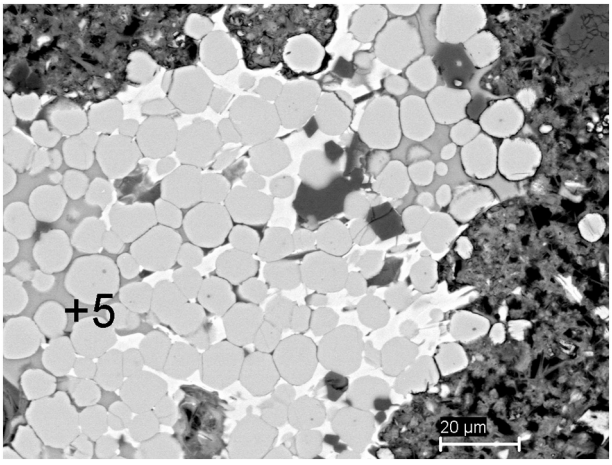

Fig. 7. CGT1: small, round C_2S crystals in a $C_{12}A_7$ (+5) and ferrite matrix; SEM-BSD.

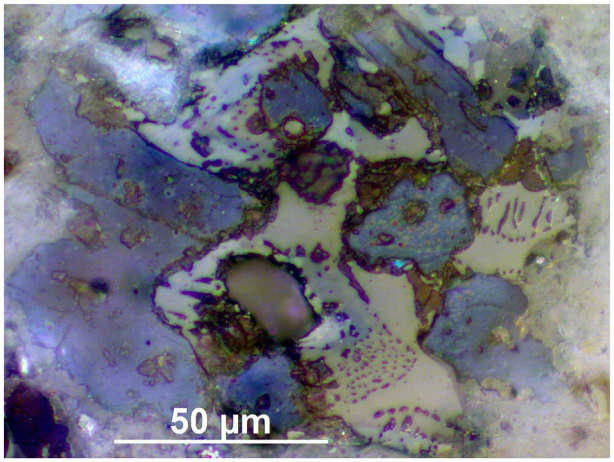

Fig. 6. CGT1: large, corroded C_3S (blue) surrounded by small, secondary C_2S crystals (brown) in coarse interstitial aluminate (grey) and ferrite (white). RL, Nital etch. (For interpretation of the references to colour in this figure legend, the reader is referred to the web version of this article.)

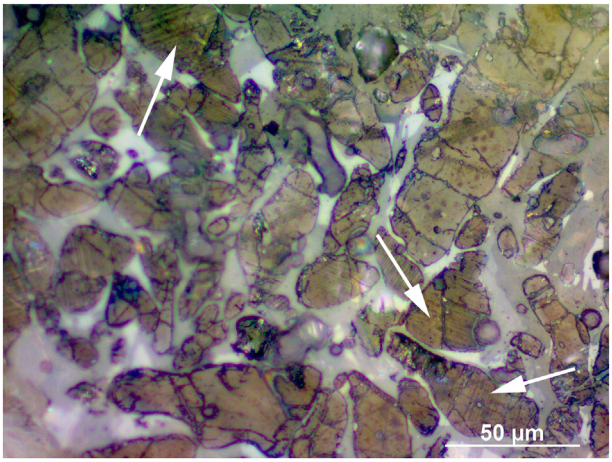

Fig. 8. CGT1: large, elongated C_2S (type II, arrows). RL, Nital etch.

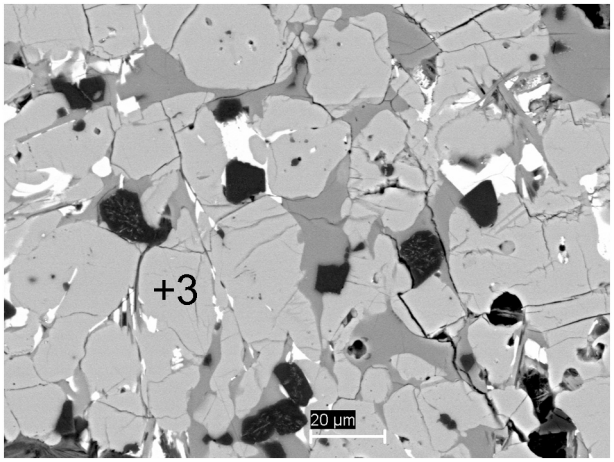

Fig. 9. CGT1: elongated C_2S (+3), coarse $C_{12}A_7$ (grey), ferrite (white) and MgO (black); SEM-BSD.

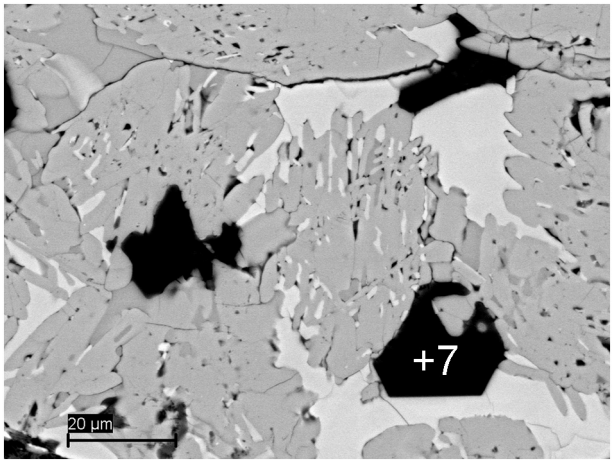

Fig. 10. CGT1: C_2S with serrated projection into interstitial ferrite and subhedral MgO (+7); SEM-BSD.

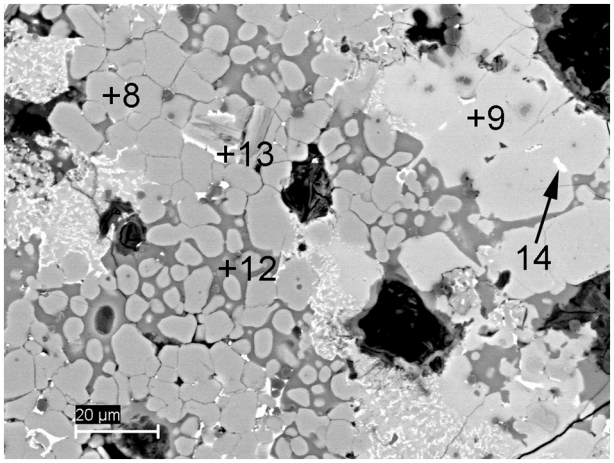

Fig. 11. CGT2: C_2S (+8), $-$C_2S (+9) with $Fe_{(1-x)}S$ (14) embedded in aluminate (+12) and ferrite (+13); SEM-BSD.

even if a low acceleration voltage was used during the measurements.

Fig. 12 shows another residue containing very fine C_2S crystals embedded in a calcium sulfosilicate solid solution exhibiting atomic ratios Ca/Si of 2.55 and Si/S of 2.03 (Table 2) and corresponding to C_5S_2\$. Small SO_3-bearing aluminate phases also exist in a few residues

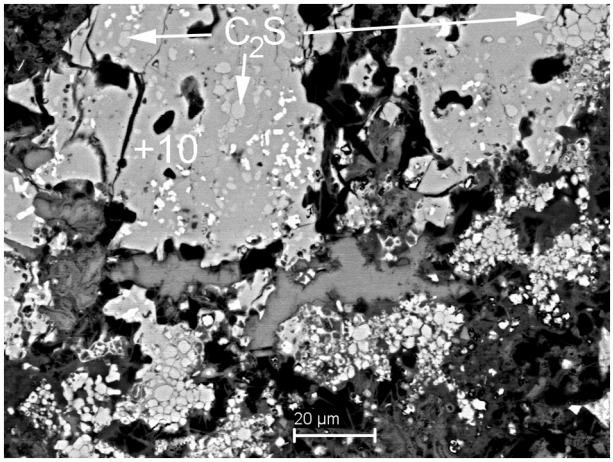

Fig. 12. CGT2: minute C_2S crystals in C_5S_2\$ (+10); SEM-BSD.

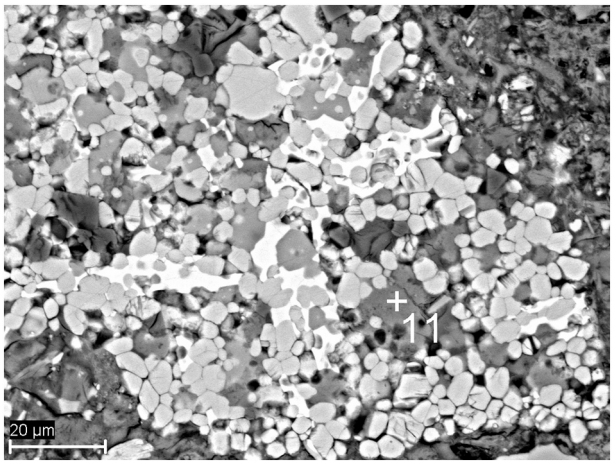

Fig. 13. CGT2: C_2S crystals with C_4A_3\$ (+11) and ferrite (white); SEM-BSD.

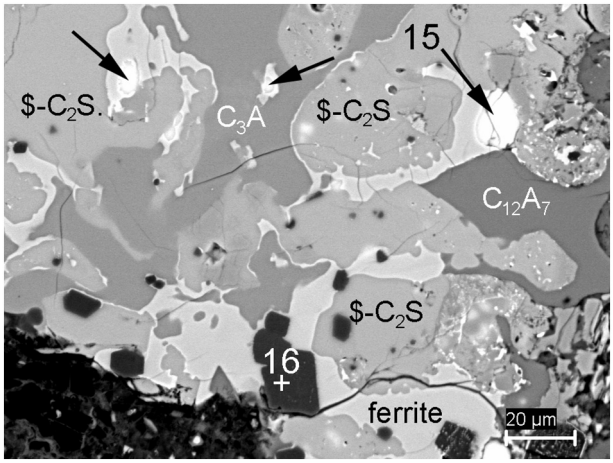

Fig. 14. CGT2: $-$C_2S, $C_{12}A_7$, C_3A, ferrite, CaS (15 and arrows), and (Mg,Fe)O (+16); SEM-BSD.

(Fig. 13), where atomic ratios Ca/Al = 0.69 and Ca/S = 3.82 (Table 2) suggest the presence of C_4A_3\$.

Furthermore, in a few residues calcium sulphide (CaS) is identified as small crystals or droplets in the vicinity of $-$C_2S (Fig. 14). Coarse crystals of flux phases rich in iron exhibit an average sulfur content of approx. 0.5 to 0.7 at.%; aluminate is present as $C_{12}A_7$ (Figs. 11 and 14), rarely in the form of C_3A (Fig. 14) containing, similarly to ferrite, low

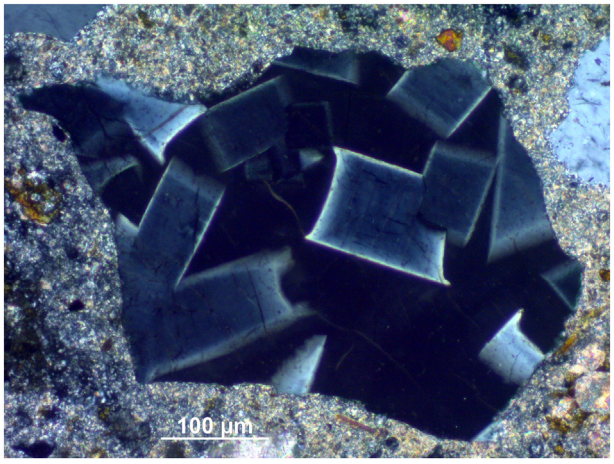

Fig. 15. CGT3: tabular, zoned melilite (predominantly C_2AS) in an amorphous matrix; TPL.

amounts of sulfur (Table 2).

On the contrary to CGT1, the polyhedral MgO crystals (Fig. 14) contain a significant amount of Fe (atomic ratios being Mg/Mg + Fe ~0.82 to 0.86; Table 2).

3.2.3. Binder-related residues containing melilite and CS (CGT3)

Fig. 15 shows large, zoned tabular crystals of melilite (predominantly C_2AS) which are embedded into an amorphous matrix. Other glassy residues contain calcium silicate laths with Ca/Si ratios of 0.95 to 0.97 corresponding to CS, wollastonite or one of its polymorphs (Fig. 16, Table 2). The absence of any hydration rims or dissolution patterns suggests their non-hydraulic nature. Cement residues with comparable composition and properties are frequently reported in low temperature (i.e. 900 to 1100 °C) RCs [3,23] and also in early PCs [14–16].

3.2.4. Low-temperature phases and residues of the raw material (CGT4)

The microstructure and composition of residues belonging to the CGT4 group indicate that their formation was connected to the lower temperature regimes of the kiln. Although there is clear evidence of $CaO\text{-}SiO_2$ interactions mostly resulting from the formation of calcium silicates (with compositions corresponding the members of the $CS\text{-}C_2S$ series), non-reacted or residual quartz, feldspar and sheet silicates, as well as carbonate (calcite, dolomite) minerals (Figs. 17 and 18) indicate the incomplete reaction due to insufficient temperatures. Very similar

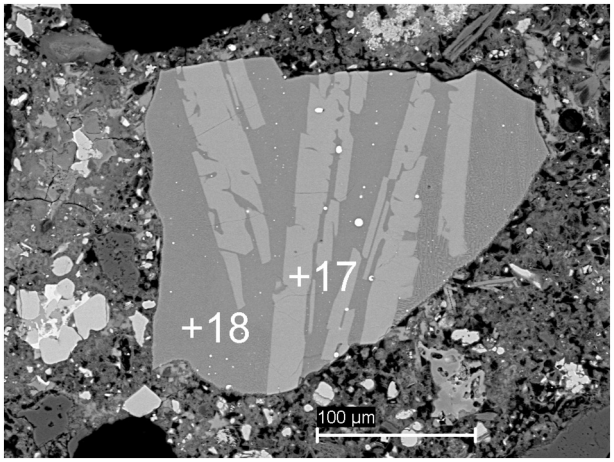

Fig. 16. CGT3: CS laths (+17) in an amorphous-glassy matrix (+18); SEM-BSD.

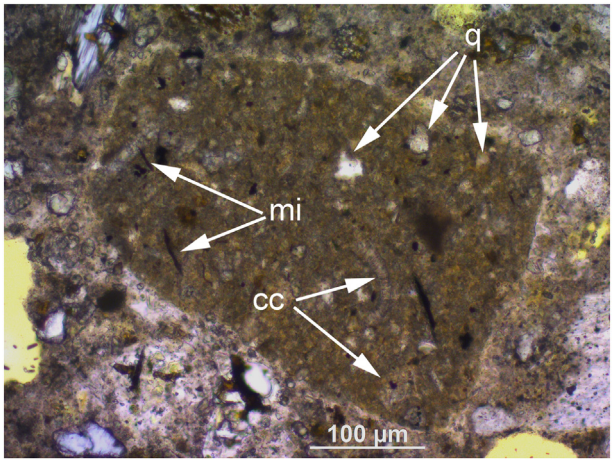

Fig. 17. CGT4: under burned residue of the raw material containing relicts of quartz (q), carbonate (cc) and sheet silicates (mi = mica); TPL.

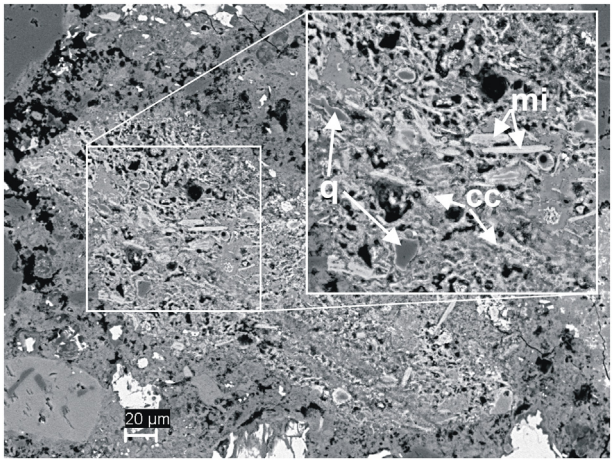

Fig. 18. CGT4: under burned residue of the raw material with relicts of quartz (q), mica (mi) and carbonate (cc) showing partially reactions due to calcination. The original rock texture is still recognizable; SEM-BSD.

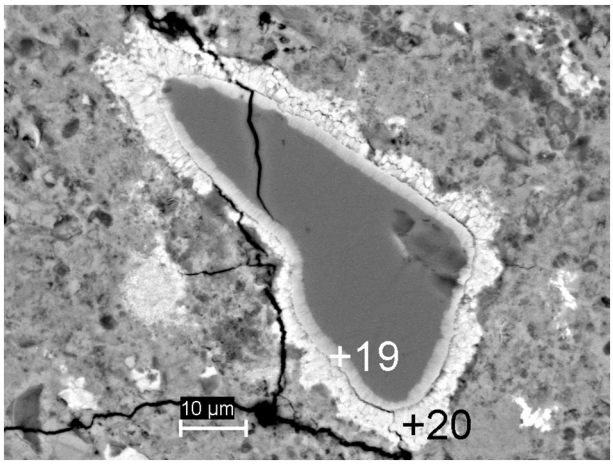

Fig. 19. CGT4: large residue of quartz with layered rim of calcium diffusion. Inner rim: CS (+19), outer rim: C_2S (+20); SEM-BSD.

composition and texture were reported [3,23] on the anhydrous binder residues of historical RCs which are normally classified into the under burned cement fractions. The analyses of the present samples also suggest the above observations: residual grains of under burned

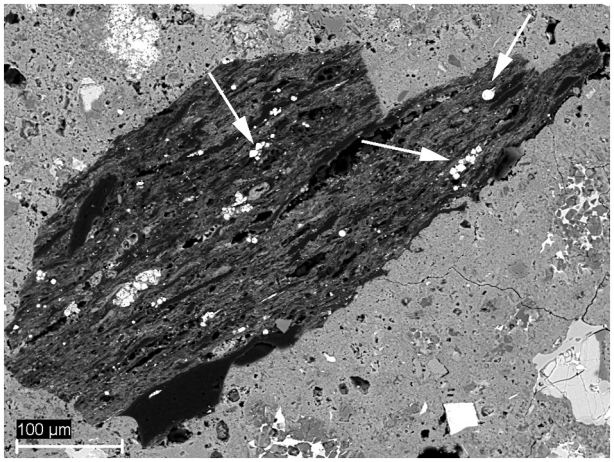

Fig. 20. Remnant of brown coal used as solid fuel for cement burning. Minute, bright inclusions (arrows) are FeS_2 crystals; SEM-BSD.

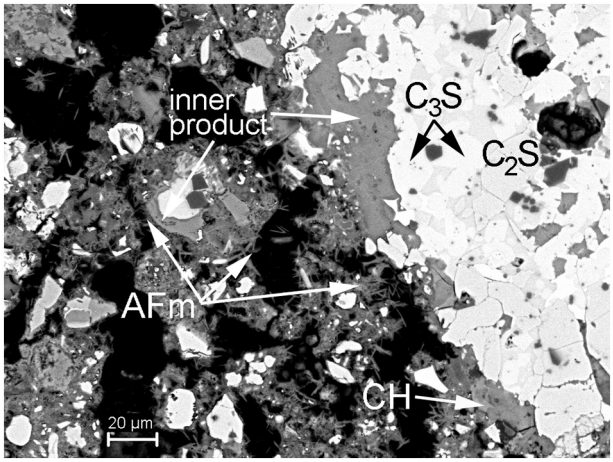

Fig. 22. Rim of inner hydration products around residual cement grains (CGT1). In the porous matrix (outer products) platy crystals of AFm phases are visible; SEM-BSD.

character preserved the original texture of the raw material and thus appear unreactive or slightly reactive only (Figs. 17 and 18).

Fig. 19 shows the relict of a large quartz grain where due to the diffusion of Ca into the grain three different zones of variable Ca/Si ratios (approx. 2 to 0) are visible: while the outer, partly hydrated rim (+20) is made up of C_2S and the inner layer (+19) has an average composition of CS (Table 2) the core is free of Ca.

3.2.5. Residues of solid fuel

Apart from the high mineralogical and textural variety of residual cements, both samples contain porous inclusions composed of carbon which can be interpreted as remnants of a solid fuel (Fig. 20). The Tertiary Häring bed near the historical cement plant in Kirchbichl is made up of a series of brown coal and, depending on the carbonate to silicate ratio in the layers, the so-called Roman, natural Portland and Portland cement marlstone strata [24,25] used for cement production since the mid 1800s [7]. The brown coal of the Häring bed had been mined since the early 1800s and its high (5.5 to 5.8 wt%) sulfur content was well-known already in that time [24,25]. Sulfur appears in the form of small authigenic, framboidal pyrite [25] crystals, which was also found to form crystal enlargements in the solid fuel residues (Fig. 20).

3.3. Composition of the hydration products

Hydration products are unevenly distributed in the binder forming in non-carbonated areas a disseminated and high microporosity. Similarly to OPC, some dense inner products (Figs. 21 and 22) that are visible at the boundary of cement grains predominantly belong to the CGT1 group and related to the hydration of C_3S. Furthermore, the presence of an inner products rim is not systematic, as illustrated by Fig. 21 showing the difference between two neighbouring grains of the CGT1 group. In these examples, the presence of C_3S is identified as the main factor influencing the development of thick hydration rim (the cement grain on the right contains only C_2S). Additionally, the outer hydration products are distributed forming a mixture of compact clusters and platy AFm phases (Fig. 22). Calcium hydroxide can be locally observed in lesser amounts either as secondary filling in air voids, or clusters of primary hydration products in the vicinity of cement grains in the sample ADM2 (Fig. 22). In contrast, the fully carbonated outer areas of the mortars sample show a dense microstructure (see Fig. 20).

Since both samples have been affected by carbonation, EDX measurements of the hydration products have only been carried out on selected areas in sample ADM2, where a few non- or just slightly carbonated binder portions have been preserved. Representative cement grains belonging to the types CGT1 and CGT2 with partly well-developed hydration rims have been chosen for the measurements, in order to compare the composition of the hydration products in the vicinity of cement grains with different compositions.

Fig. 23 shows the distribution of the EDX atomic ratio of the inner and outer hydration products.

The composition of the inner products (Fig. 23a and b) partly overlaps with that of the outer products, independently of the type of hydrated cement grain analyzed. No significant difference has been found in the nature of the hydration products between the close region of the cement grains of type CGT1 and CGT2. The data are very scattered and make the exact intermixing difficult to identify. The inner products are composed of a mixture of C-S-H and AFm (monosulfoaluminate and monocarboaluminate), in which ettringite is detected in insubstantial amounts. Dots of hydration products with high (0.80 to 0.95) Si/Ca and low (0.04 to 0.18) Al/Ca ratios (Fig. 23a) refer to the presence of hydrous silica in the carbonated C-S-H. The outer products (Fig. 23c and d) contain very low amounts of AFm as well as very little ettringite and the values also indicate the partly carbonation of C-S-H and CH (Fig. 23c). It is notable that the outer products contain less sulfo-AFm/AFt than the inner products, contrary to the usual SEM observations made on modern PC systems.

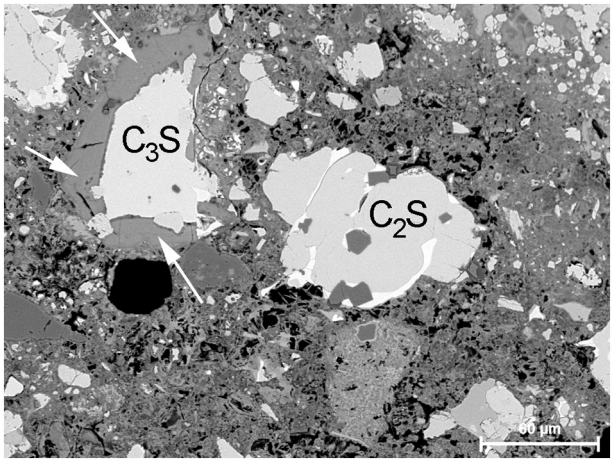

Fig. 21. Residual cement grains (CGT1) with (arrows) and without well-developed rim of inner hydration products; SEM-BSD.

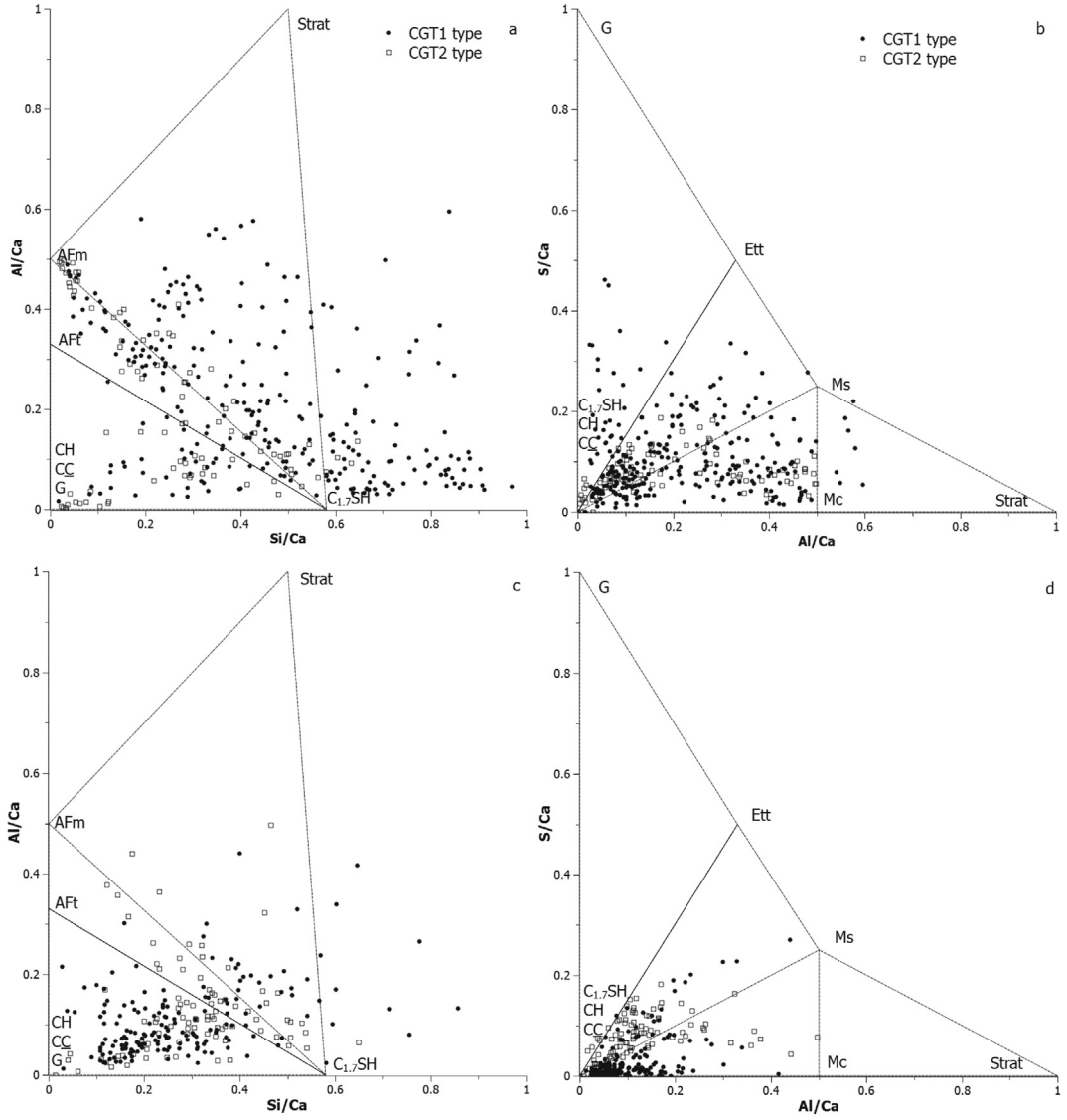

Fig. 23. EDX data of representative inner (a and b) and outer hydration products (c and d) measured around cement grains belonging to CGT1 and CGT2, respectively. Values are expressed as atomic ratios of Al/Ca, Si/Ca and S/Ca compared to stoichiometric C-S-H, AFt (ettringite: Ett), AFm (monosulfoaluminate: Ms., monocarboaluminate: Mc), strätlingite (Strat), calcium hydroxide (CH), calcium carbonate (C$\underline{C}$), and gypsum (G).

4. Discussion

4.1. Diversity and thermal history of cement minerals and binder-related phases

The optical appearance and mineralogical composition of the majority of the residual cement grains correspond to other 19th century PCs described in former studies [1,2,9–17] indicating the characteristics of historical cement production such as inhomogeneous raw materials, slow heating and cooling rates, hot spots in the kiln, etc. Yet some specific phases found in the samples have not been previously reported in historical PCs. Regarding the general mineralogical composition, approximately three-fourths of the residues have a PC character, though with a dominance of C_2S over C_3S, which suggest a suboptimal composition (i.e. less CaO compared to silica and aluminates) in the natural raw material. The average large size (40 to 60 μm) of C_3S crystals, typical for shaft or bottle kiln burning, is a result of a long burning with low gradient of temperature and/or burning at high temperatures [5,15,26]. Furthermore, the coalescence of C_3S also suggests low heating rates [15,16,26]. C_3S grains surrounded by C_2S crystals indicate that CaO was consumed by the flux upon cooling resulting in the corrosion of the surface of the C_3S grains and the crystallization of secondary C_2S [27]. While the reaction is promoted by higher alumina ratios [28], the smooth surface of the C_3S and secondary C_2S refer again to slow cooling [27].

Similarly to C_3S the diversity of C_2S crystal habits and textures also suggests various burning temperatures, times of residence and cooling rates. The formation of type I cross lamellae in a few C_2S grains observed in both samples is an indication of α-α′ inversion taking place at high temperatures (i.e. above 1430 °C) and followed by slow cooling [5,15,16]. Since the crystal size of C_2S is primarily dependent on the burning time, the unusually large crystals of elongated, wedge-shaped habits indicate temperatures (i.e. above 1400 °C) maintained for a long time where single crystals had enough time to grow in the fluid [5]. For sufficient time at high temperature α′ C_2S grows into coarse crystals of α C_2S due to recrystallization. During cooling the α C_2S transforms to the α′ polymorphs and later (at around 700 °C) to β C_2S, which is characterized by one set of parallel lamellae (type II) or without lamellae (type III) [16]. Therefore, the above mentioned C_2S habits are characteristic components, as reported in over burned early PC clinkers produced in bottle or shaft kilns [15,16]. Conversely, minute and round type III C_2S, 5 to 20 μm in diameter signify that their formation took

place in the lower temperature regimes of the kiln [2]. Although C_2S is generally more stable than C_3S upon slow cooling it can exhibit re-absorbed finger-like pattern within the interstitial phases [5,29], as observed in some of the CGT1 residues. Finally, C_2S nests indicate inhomogeneities which can be lead back to the presence of larger quartz crystals in the raw material [5,30].

The coarse aluminate and ferrite phases are also consistent with very slow cooling. Besides C_3A, $C_{12}A_7$ was also detected in a smaller portion of residues. Although $C_{12}A_7$ normally melts above 1250 °C [31,32], in PC it may coexist with C_3A from 1000 °C up to 1400 °C in the case of higher alumina ratios [32]. The co-existence of both phases was observed in several cement residues along with the fact that aluminates dominate over the ferrite phases which also indicates the use of a raw material richer in alumina (i.e. clay minerals) [31] compared to accurately by-mixed raw meals used in OPC. The presence of Mg-rich C_2S [30] and the fact that many cement grains contain MgO or (Mg,Fe)O refer to dolomitic impurities in the raw material. Schulz et al. [25] describe the interbedding of dolomite and dolomitic limestone strata in the Häring beds as possible source of Mg during cement production.

The minerals containing variable amounts of SO_3 indicate the influence of an external and/or an internal source of sulfur. The first one was verified in the form of FeS_2 impurities in the brown coal residues. The second one was detected in the vicinity of the \$-C_2S as minute $Fe_{(1-x)}S$ and CaS, which are interpreted as newly formed phases caused by the decomposition of the FeS_2 in the marlstone during burning.

During the thermal decomposition of FeS_2 sulfur vapour was released [33] and combined with the clinker minerals. If the amount of alkalis is high, SO_3 preferentially forms alkali sulfates; otherwise it predominantly enters the structure of C_2S [34]. In the present samples a maximum content of 3.7 wt% of SO_3 has been detected, which is much above that observed in OPCs [32]. Further interaction of SO_3 with C_2S resulted in the formation of small amounts of C_5S_2\$. For the formation of C_5S_2\$ in presence of C_2S or CS, an excess of calcium sulfate, temperatures around 1200 °C and a slow cooling rate are required [35]. We assume however, that the FeS_2 impurities in the raw material acted similarly to calcium sulfate observed in the laboratory experiments.

Besides sulfosilicates, C_4A_3\$ has also been verified as a minor component in the CGT2 residues being a common component in modern CSA and BSA cements [36]. To avoid its decomposition, the clinkering temperature should not be higher than 1350 °C [36]; consequently, its formation is connected to a lower burning zone temperature (~1250 °C) in modern kilns [36]. Similarly to C_5S_2\$-bearing residues, cement grains that contained C_4A_3\$ were also free of C_3S suggesting the above mentioned lower temperature regime of formation. A recent study mentions the presence of C_4A_3\$ traces in 1880 PC cement mortar samples [37]. Finally, CaS verified in the samples has been reported as a minor component in blast furnace slag [38,39], but it may also form in OPCs when during burning reducing atmosphere develops [28,40].

The distribution of SO_3 in the residues is variable, but affects only a minor amount of the total cement clinker minerals. Taking into consideration the existence of its possible sources, two different types of processes can be assumed in the kiln between the FeS_2 and the mineral components of the raw material.

First, the presence of FeS_2 in the marlstone has enabled the direct formation of \$-C_2S and other SO_3-bearing cement phases as a consequence of the reaction between the iron sulphide, silica, clay minerals and calcium carbonate [41]. However, due to the decomposition of FeS_2 on elevated temperatures its previous existence in the marlstone can only be assumed by the presence of newly formed $Fe_{(1-x)}S$ and CaS, as observed in some CGT2 grains.

Secondly, the oxidation of FeS_2 in the coal resulting in the release of SO_3 and distributed by vapour-phase transport in the kiln [42] may also react with the different calcium silicates and flux phases to produce SO_3-bearing cement minerals.

The formation of C_5S_2\$ via sulfur combustion was also reported as a minor phase in belite rich CSA cements [43], supporting our observations (see Fig. 12) and hypothesis on the formation of C_5S_2\$ by the direct reaction between C_2S and SO_3. Based on recent thermodynamic calculations [44] the upper limit stability temperature of C_5S_2\$ can be given as app. 1290 °C. This limit is not fixed and depends on the gas fugacity [44], although most authors give the stability temperature range between 900 and 1200 °C [45]. Cement residues containing C_5S_2\$ were found to be free of C_3S which also suggests that they were formed in kiln zones where the temperature was not sufficiently high to form C_3S.

SO_3 content may be highly variable in modern kilns ranging from almost zero to several percent when sulfur-rich fuels are used [44], but this variability might be even more significant in historical shaft kilns. Their size, geometry, the placement of raw feed and fuel in layers [6] and their long burning time induced not only an inhomogeneous distribution of heat, but also a high variability of SO_2 partial pressure. The exact determination of these parameters based on historical cement mortars is beyond the scope of this study; the low amounts of SO_3-bearing cement phases suggest however, that the conditions such as the amount of FeS_2 impurities in the raw material, the SO_2 partial pressure, the temperature and the phase composition for the optimal formation were limited and only occasional.

CS and C_2AS are typical components in historical cements [3,15,23,31] as they formed from minerals rich in silica and alumina (i.e. clay, feldspars), respectively. Even though these phases belong to a class of cement minerals that exhibit very low-reactivity and thus remain unhydrated after almost 150 years in atmospheric conditions with no prolonged contact with water, they provide information about the reactions taking place in the moderate temperature regime (i.e. 800 to 1100 °C) of the kiln [23].

Finally, the under burned particles preserving the original texture of the raw material confirm the assumption about the use of a natural rock that contained the necessary mineral components in intimate mixture for the cement production. Such residues witness the zones of lowest temperature during the burning process. Recent data on calcination tests carried out on RCs [46] can be used to compare the present samples and estimate the possible lowest temperature of calcination. The grains containing residues of calcium carbonate and silica with traces of calcium diffusion rims or little amount of C_2S may not have exceeded 700 to 800 °C. Remnants of large quartz grains exhibiting partly hydrated rims made up of C_2S are not only the witnesses of insufficient reactions, but, similarly to the C_2S nests observed in the CGT1, also inhomogeneous raw material. The silty-sandy interbeddings in the Häring cement-layers [25] reflect the natural diversity of the source rock.

Considering the co-existence of cement residues which reflect extremely different thermal histories (from under burned at approx. 750 °C up to over burned PC residues at > 1400 °C), the question arises whether they could have formed within the same batch simultaneously, or their co-existence suggest that different batches were mixed up for delivery. Due to the lack of historical data concerning the early Austrian PC production techniques this question cannot be answered unambiguously. Some general consideration can however be made. The overgrowth of wedge-shaped C_2S indicates that a part of the clinker was exposed to high temperatures for long time during calcination. However, it's amount is lower compared to the clinker minerals formed at lower temperatures (i.e. 1100–1300 °C), which suggests the existence of hot spots [47], where over burned C_2S crystals could grow in the liquid due to the highest temperature (i.e. > 1400 °C [15]) and long time of residence. The production of PCs in the 1860s took place in rebuilt discontinuous RC shaft kilns [2,6]. To get an idea about their dimension, RC shaft kilns in Austria from the same period can be assumed as comparable structures with an average height of 8 m and a diameter of 2 to 3 m [6]. It is admitted, that due to the size, geometry and way of operation wide range of temperatures up to 600 °C differences within one batch [48] may exist both in historical and modern

shaft kilns. The difference of clinker mineralogy, as a function of the temperature distribution, has been recently reported in modern RCs produced in a small size test kiln [49], in which a temperature gradient from 840 °C (measured internal boundary wall) to 1140 °C (in the centre of the kiln) can directly influence, for instance, the ratio of α′ to β-C_2S. Furthermore, the raw material (marlstone) and fuel (brown coal) was alternating filled into the kiln and burned for several days, afterwards the coarse clinker was sorted, where the over and under burned portions had been removed from the batch [6]. This, so-called discontinuous burning procedure was adopted from RCs [6] and confirms the observations on the low amounts of under burned (CGT3 and 4) cement residues. A recent study on historical PCs from Japan [16] has reported that in certain cement plants the under burned clinker was calcined again as a raw material. Although there is no reference available to the same technique in Austria, we cannot unambiguously exclude this possibility either. It has to be mentioned however, that the further re-burning of under burned clinkers might have resulted in higher amounts of wedge-shaped C_2S formed at high temperature and also under burned residues to a lesser extent.

4.2. Hydration mechanisms

In OPC, the development of the inner products is a long term reaction mostly related to the formation of C-S-H from the boundary to the core of the grains [32]. In the present samples the formation of the inner rim seems to be related predominantly to the C_3S presence in the grains. Other cement residues containing C_2S only do not show any well-developed hydration rim. The sulfate-bearing phases concentrate in the inner products rather than in the outer ones, unlike in the case of modern OPC hydration which might be a result of a combination of mechanisms. First, since the use of interground calcium sulfate as a setting retarder can be excluded [6], the sulfur in the anhydrous cement was present in low reactive $C_5S_2\$$, $C_4A_3\$$, CaS and predominantly $\$$-C_2S. Consequently, sulfate availability would be very limited in the early stages of hydration and so monosulfoaluminate and in particular ettringite would have been scarce. In addition, due to the assumed surplus of aluminium in the raw material, AFm might form as a mixture of hydroxy-AFm and some monosulfoaluminate. Aluminate was identified in the form of crystalline C_3A, $C_{12}A_7$ and ferrite observed in CGT1 and 2, and as non-reactive C_2AS in the CGT3 grains. Amorphous aluminate, frequently found in RCs [50], in the CGT4 grains cannot be excluded either, but its evidence in the samples remains difficult to confirm. Furthermore, hydroxy-AFm is unstable [51] and converts, depending on the availability of other anions, to monosulfoaluminate and/or monocarboaluminate.

Finally, the coarse grain size distribution is one of the main factors reducing the availability of both aluminate and sulfate to form typical sulfo-AFm/AFt. As mentioned above, the phases containing sulfur have a low rate of dissolution. $C_5S_2\$$ alone has been considered as slightly reactive and its formation at the expense of the more reactive $C_4A_3\$$ has been avoided throughout the development of BSA cements [36]. Nonetheless, $C_5S_2\$$ can be reactive under certain conditions, e.g. in presence of aluminium hydroxide [45] to form strätlingite and C-S-H. In the near surface of the present cement grains containing $C_5S_2\$$ (CGT2), strätlingite has not been detected by EDX, indicating its scarcity.

The existence of monocarboaluminate shows that the monosulfoaluminate underwent carbonation during the service life of the mortar. During carbonation sulfate is released from monosulfoaluminate, which can form additional ettringite [51]. However, it is not possible to determine whether the insignificant amount of AFt detected in the binder was formed due to carbonation of monosulfoaluminate, by additional release of sulfate from cement grains, or it was a consequence of external sulfate sources.

Unlike modern OPC the initial precipitation of ettringite, responsible for the setting regulation, would not have occurred in the present cements, due to the lack of additionally by-mixed calcium sulfate. In practice, the setting time was probably regulated by a technique mentioned by Pierus [6]; before milling the clinker was stored in a hut for several days, where atmospheric humidity reacted and deactivated to some extent the cement phases (i.e. C_3A and probably also amorphous aluminates) responsible for prompt setting. The deactivation of the initial flash setting, by pre-wetting the sand up to 12 wt% of the total mixing water, has been experienced [52] on a range of modern rapid natural cements. This simple technique allows a significant increment of the setting time (even for prolonged storage of pre-wet mixes) and does not cause any detrimental influence on the strength and shrinkage. Additionally, slow cooling can also alter the chemical characteristics and crystal lattice distortion of the clinker phases resulting in less reactive cement [29].

Microscopic observations indicate a relatively high capillary porosity in both samples (see Figs. 7, 12, 16, 21 and 22) with the exception of the areas subjected to carbonation. Consequently, the origin of this pore structure can be suggested by the development of poorly-packed hydrate phases resulting from three main parameters:

i) the coarse particle size distribution of the cement grains leading, along with the above mentioned historical deactivation technique, to a relatively low reactivity and uneven distribution of different hydration products;
ii) the heterogeneous distribution of the calcium silicates and relatively low amount of C_3S within the reactive cement grains and subsequent distribution of C-S-H;
iii) as a consequence of i) and ii), extra water to ensure the workability of mortar not taking part in the hydration and contributing to the development of capillaries.

In the present samples these parameters seem to control the development of capillary structure. However, and contrary to modern PC concrete and mortars, the high capillary porosity is not apparently involved in any durability issues. Indeed the samples and the whole façade do not show any degradation patterns, except for carbonation, directly related to the interaction of the environment and the capillary structure of the mortars. Moreover, the presumably limited amount of calcium hydroxide might have also contributed to reducing the durability issues related to the long term process of dissolution and precipitation of salts (e.g. ettringite or gypsum from atmospheric sulfation). These properties of durability are closely comparable to those of RC mortars reported for their long lasting behavior [53,54].

5. Conclusions

One of the earliest documented (1866 to 1870) natural Portland cement applications in Austria was studied. Based on the investigation of cement residues and hydration products of two mortar samples the following conclusions can be drawn:

- The binder was a natural Portland cement burned in a vertical shaft kiln. Approx. 3/4 of the unhydrated cement residues have a PC feature, whose size, amount and mineralogical composition reflect a long time of burning and residence and a slow cooling rate. Large and elongated C_2S crystals indicate high temperature (> 1400 °C) of formation, suggesting the existence of hot-spots in the kiln. Cement minerals such as CS, C_2AS and under burned raw material residues suggest kiln zones with much lower temperatures (approx. 700 to 1100 °C) and thus indicate a very uneven heat distribution during calcination. Under burned raw material residues are useful witnesses to confirm the original raw material, which was in the case of this cement a natural marlstone.
- The presence of sulfur-bearing cement residues can be traced back to the use of a local pyrite-bearing marlstone as raw material and brown coal as a solid fuel containing FeS_2. During the burning SO_3 has been released and combined with mineral components which

resulted in the formation of limited amounts of sulfosilicates, sulfoaluminate and CaS.

- The distribution pattern of hydration products show the low amounts of sulfo-AFm and AFt phases predominantly concentrated in the inner products atypical for modern OPC and confirming the absence of by-mixed calcium sulfate as a setting retarder. Sulfo-AFm phases may be connected to later stages of hydration caused by the dissolution of sulfur during the hydration of calcium sulfosilicates. Monosulfoaluminate is partly carbonated to form monocarboaluminate in the inner products.
- The working time of the mortar was positively influenced by the coarse grain size of the cement and the presumable application of a deactivation method applied on the clinker by storing it under atmospheric conditions for a certain time.
- Unlike modern OPC-based mortars the above parameters seem to have influenced the development of a capillary structure which is not apparently involved in any durability issues and has resulted in a very good state of preservation after 150 years of atmospheric exposure.

Acknowledgements

The authors are gratefully acknowledge Karl Stingl (Association for the Advancement of the Architectural Heritage Conservation, Austria) for his invaluable help in sampling and providing information about the development and use of historical Portland cements in Austria as well as Nicholas B Winter (WHD Microanalysis Consultants Ltd., UK) and Anthony Baragona (University of Applied Arts, Austria) for their critical comments on the manuscript.

References

[1] R.G. Blezard, The history of calcareous cements, in: P.C. Hewlett (Ed.), Lea's Chemistry of Cement and Concrete, fourth ed., Elsevier, Oxford, 2006, pp. 1–23.
[2] R.G. Blezard, Reflections on the history of the chemistry of cement, SCI Lecture Papers Series, Society of Chemical Industry, 1998(27p).
[3] J. Weber, K. Bayer, F. Pintér, 19th century ´novel´ building materials: examples of various historic mortars under the microscope, in: J. Válek, J.J. Hughes, C.J.W.P. Groot (Eds.), Historic mortars: Characterization, Assessment and Repair, RILEM 7, Springer, 2012, pp. 89–103.
[4] J. Weber, N. Gadermayr, K. Bayer, D. Hughes, R. Kozłowski, R. Stillhammerova, D. Ullrich, R. Vyskocilova, Roman Cement Mortars in Europe's Architectural Heritage of the 19th Century, J. ASTM Int. 4 (2007) (Paper ID JAI100667).
[5] D.H. Campbell, Microscopical Examination and Interpretation of Portland Cement and Clinker, Portland Cement Association, Skokie, 1999.
[6] T. Pierus, Ueber die Fabrikation von Roman- und Portland-Cement, Pierus Verlag, Wien, 1900.
[7] F. Kirchmair, Schwoich – die Wiege der österreichischen Zementindustrie, in: F. Kirchmair (Ed.), Das Schwoicher Dorfbuch, OSR Verlag, 1988, pp. 83–100.
[8] K. Zechetner, Zementwerke in Niederösterreich, in: G. Lindner (Ed.), Beton, Denkmalpflege in Niederösterreich, Amt der NÖ Landesregierung, 2010, pp. 20–21.
[9] R.G. Blezard, Technical aspects of Victorian cement, Chem. Ind. (1981) 630–636.
[10] G.M. Idorn, N. Thaulow, Examination of 136-years-old Portland cement concrete, Cem. Concr. Res. 13 (1983) 739–743.
[11] K.L. Scrivener, A study of the microstructure of two old cement pastes, Proceedings of the 8th ICCC, Rio De Janeiro, 1986, pp. 389–393.
[12] T. Katayama, K. Sarai, Petrography of 100-year-old concrete from Otaru port, Japan, Proceedings of the 2nd International Conference on Concrete Under Severe Conditions (CONSEC' 98) Tromsø, Norway, 1998, pp. 250–261.
[13] K. Peterson, L. Mailloux, L. Sutter, Regressions in Portland cement clinker microscopy – clinker from 1906: a snapshot of the early American Portland cement and road construction industries, Proceedings of the 34th ICMA Conference, Halle, Germany, April 1–4, 2012 (12p).
[14] F. Pintér, T. Köberle, J. Weber, Composition and properties of a historic Portland cement mortar from 1879: a microscopic study, Proceedings of the 14th EMABM Conference, June 10–14, 2013, p. 10 Helsingør, Denmark.
[15] Y. Ando, S. Hirono, D. Sawaki, T. Katayama, Microscopy to evaluate the properties of cement and alterations in historic mortar/concrete of old Nobiru Port project, Northeast Japan, Proceedings of the 36th ICMA Conference, Milan, Italy, April 13–17, 2014, pp. 212–233.
[16] T. Katayama, Y. Ando, S. Hirono, D. Sawaki, H. Itoga, Relicts of unhydrated cement clinker in a historic concrete from the 19th century – microscopy with EDS analysis of old training dyke at Yokohama port, Japan, Proceedings of the 36th ICMA Conference, Milan, Italy, April 13–17, 2014, pp. 432–458.
[17] F. Pintér, C. Gosselin, Material characteristics of prefabricated concrete elements from a late 19th century church in Lower Austria, Proceedings of the 15th EMABM Conference, June 17–19, 2015, pp. 131–138 Delft, The Netherlands.
[18] J. Wichner, Kloster Admont in Steiermark und seine Beziehungen zur Kunst, R, Brezezowksy und Söhne, Wien, 1888.
[19] J.A. Janisch, Topographisch-statistisches Lexikon von Steiermark mit historischen Notizen und Anmerkungen, Leylam-Josefstahl, Graz, 1878.
[20] H. Insley, Structural characteristics of some constituents of Portland cement clinker, J. Res. Natl. Bur. Stand. 17 Research Paper RP917, Washington D.C., 1936, pp. 353–361.
[21] H.G. Midgley, M. Bennett, A microprobe analysis of Larnite and Bredigite from Scawt Hill, Larne, Northern Ireland, Cem. Concr. Res. (4) (1971) 413–418.
[22] H. Pöllmann, Calcium aluminate cements: raw materials, differences, hydration and properties, Rev. Mineral. Geochem. 74 (2012) 1–82.
[23] J. Weber, N. Gadermayr, R. Kozłowski, D. Mucha, D. Hughes, D. Jaglin, W. Schwarz, Microstructure and mineral composition of Roman cements produced at defined calcination conditions, Mater. Charact. 58 (2007) 1217–1228.
[24] L. Weber, A. Weiss, Bergbaugeschichte und Geologie der österreichischen Braunkohlvorkommen, Geologische Bundesanstalt, Wien, 1983.
[25] O. Schulz, H.W. Fuchs, Kohle in Tirol: Eine historische, kohlenpetrologische und lagerstättenkundliche Betrachtung, Arch. f. Lagerst. Forsch. Geol. BA 13 (1991) 123–213.
[26] Y. Ono, S. Kawamura, Y. Soda, Microscopic Observations of Alite and Belite and Hydraulic Strength of Cement, 5th, Int. Symp. Chem. Cement, Tokyo, 1968, pp. 275–284.
[27] M. Böhm, A. Knöpfelmacher, R. Pierkes, Alite Decomposition Vs. Alite Corrosion, Proceedings of the 17th EMABM Conference, 14–18 May 2017, Les Diablerets, Switzerland, (2017), pp. 23–26.
[28] F. Gille, I. Dreizler, K. Grade, H. Krämer, E. Woermann, Mikroskopie des Zementklinkers, Bilderatlas, Association of the German Cement Industry, Beton Verlag, Düsseldorf, Germany, (1965).
[29] T. Sibbick, J. Cheung, The use of cement clinker microscopy as an aid to determine the performance differences in the presence of chemical additives, Proceedings of the 36th ICMA Conference, Milan, Italy, April 13–17, 2014, pp. 191–211.
[30] F.P. Glasser, The burning of Portland cement, in: P.C. Hewlett (Ed.), Lea's Chemistry of Cement and Concrete, fourth ed., Elsevier, Oxford, 2006, pp. 195–240.
[31] P. Daritz, J. Neubauer, F. Goetz-Neunhoeffer, T. Schmid, Calcium aluminates in clinker remnants as marker phases for various types of 19th-century cement studied by Raman microspectroscopy, Eur. J. Mineral. 28 (2016) 907–914.
[32] H.F.W. Taylor, Cement Chemistry, second ed., Academic Press, London, 1990.
[33] Y. Hong, B. Fegley Jr., The kinetics and mechanism of pyrite thermal decomposition, Berichte der Bundesgesellschaft für physikalische Chemie 101 (1997) 1785–1968.
[34] A. Gies, D. Knöfel, Influence of sulfur on the composition of belite-rich cement clinkers and the technological properties of the resulting cements, Cem. Concr. Res. 17 (1987) 317–328.
[35] M.B. Haha, F. Bullerjahn, M. Zajac, On the reactivity of ternesite, Proceedings of the 14th International Congress on the Chemistry of Cement (ICCC), Beijing, October 13–16, 2015.
[36] M.C. Martín-Sedeño, A.J.M. Cuberos, Á.G. De la Torre, G. Álvarez-Pinazo, L.M. Ordónez, M. Gateshki, M.A.G. Aranda, Aluminum-rich belite sulfoaluminate cements: clinkering and early age hydration, Cem. Concr. Res. 40 (2010) 359–369.
[37] V. Thiéry, T. Katayama, Y. Ando, G. Link, M. Bouichou, E. Marie-Victoire, Preliminary study of 19th century mortars from railway Engineering structures abandoned since 1950, Proceedings of the 17th EMABM Conference, 14–18 May, 2017, 2017, pp. 136–139 Les Diablerets, Switzerland.
[38] N.M. Piatak, R.R. II Seal, Mineralogy and environmental geochemistry of historical iron slag, Hopewell Furnace National Historic Site, Pennsylvania, USA, Appl. Geochem. 27 (2012) 623–643.
[39] K.W. Peterson, D.M. Hammerling, L.L. Sutter, T.J. VanDam, G.R. Dewey, Oldhamite: not just in meteorites, Proceedings of the 21st ICMA Conference, Las Vegas, Nevada, USA, April 25–29, 1999, pp. 394–405.
[40] A.R. Nielsen, M.B. Larsen, P. Glarborg, K.D. Johansen, Sulfur release from cement raw materials during solid fuel combustion, Energy Fuel 25 (9) (2011) 3917–3924.
[41] D.I. Biggs, C.G. Lindsay, High temperature interactions among minerals occurring in coal, in: K.S. Vor (Ed.), Mineral Matter and Ash in Coal ACS Symposium Series, 301 1986, pp. 128–137.
[42] Y.B. Pliego-Cuervo, F.P. Glasser, The role of sulphates in cement clinkering: subsolidus phase relations in the system CaO-Al_2O_3-SiO_2-SO_3, Cem. Concr. Res. 9 (1979) 51–56.
[43] T. Hanein, I. Galan, A. Elhoweris, S. Khare, S. Skalamprinos, G. Jen, M. Whittaker, M.S. Imbabi, F.P. Glasser, M.N. Bannerman, Production of belite calcium sulfoaluminate cement using sulfur as a fuel and as a source of clinker sulfur trioxide: pilot kiln trial, Adv. Cem. Res. 28 (2016) 643–653.
[44] T. Hanein, I. Galan, F.P. Glasser, S. Skalamprinos, A. Elhoweris, M.S. Imbabi, M.N. Bannerman, Stability of ternesite and the production at scale of ternesite-based clinkers, Cem. Concr. Res. 98 (2017) 91–100.
[45] F. Bullerjahn, D. Schmitt, M.B. Haha, Effect of raw mix design and of clinkering process on the formation and mineralogical composition of (ternesite) belite calcium sulphoaluminate ferrite clinker, Cem. Concr. Res. 59 (2014) 87–95.
[46] D.C. Hughes, D. Jaglin, R. Kozłowski, D. Mucha, Roman cements - Belite cements calcined at low temperature, Cem. Concr. Res. 39 (2009) 77–89.
[47] K. Callebaut, J. Elsen, K.V. Balen, W. Viaene, Nineteenth century hydraulic restoration mortars in the Saint Michael's Church (Leuven, Belgium) - Natural hydraulic lime or cement? Cem. Concr. Res. 31 (2001) 397–403.
[48] D. Sommain, Prompt natural cement the Roman cement of Grenoble, CTLV GROUPE VICAT Liants Speciaux, Grenoble, 2007.
[49] C. Gosselin, Composition and hydration of some Roman (natural) cements, in:

R. Mangabhai, P. Hewlett, P. Domone, G. Taylor, E. Trout, D. Killoran, I. Berrie (Eds.), Institute of Concrete Technology Year Book 2013–2014, 2012, pp. 64–72.
[50] C. Gosselin, K.L. Scrivener, S.B. Feldman, W. Schwarz, The hydration of modern Roman cements used for current architectural conservation, in: J. Válek, J.J. Hughes, C.J.W.P. Groot (Eds.), Historic Mortars - Characterization, Assessment and Repair, RILEM 7, Springer, 2012, pp. 297–308.
[51] T. Matschei, B. Lothenbach, F.P. Glasser, The AFm phase in Portland cement, Cem. Concr. Res. 37 (2007) 118–130.
[52] V. Starinieri, D.C. Hughes, C. Gosselin, D. Wilk, K. Bayer, Pre-hydration as a technique for the retardation of Roman cement mortars, Cem. Concr. Res. 46 (2013) 1–13.
[53] F. Pintér, I. Vidovszky, J. Weber, K. Bayer, Mineralogical and microstructural characteristics of historic roman cement renders from Budapest, Hungary, J. Cult. Herit. 15 (2014) 219–226.
[54] C. Gosselin, F. Girardet, S.B. Feldman, Compatibility of Roman cement mortars with gypsum stones and anhydrite mortars: The example of Valère Castle (Sion, Switzerland), Proceedings of the 12th International Congress on the Deterioration and Conservation of Stone, New York, October 22–26, 2012.